

Article

Graphene Oxide Adsorption Enhanced by Attapulgite to Remove Pb (II) from Aqueous Solution

Bigui Wei ^{*}, Xiabing Cheng, Gang Wang, Hua Li, Xiaosan Song and Liang Dai ^{*}

School of Environmental and Municipal Engineering, Lanzhou Jiaotong University, Lanzhou 730070, China; gangw99@mail.lzjtu.cn (G.W.); songxs@mail.lzjtu.cn (X.S.)

^{*} Correspondence: weibg@mail.lzjtu.cn (B.W.); dailiang818@mail.lzjtu.cn (L.D.)

Received: 9 March 2019; Accepted: 28 March 2019; Published: 2 April 2019



Abstract: To improve the adsorption and separation efficiency of lead-containing wastewater by graphene oxide (GO), attapulgite (ATP) was used through a simple hydrothermal reaction. The prepared GO was characterized by SEM, TEM, FTIR, and XPS. The adsorption properties of the prepared GO were investigated. The maximum adsorption capacity of Pb²⁺ on as-prepared GO at pH 5 and 25 °C was 450.9 mg/g. It is concluded that the as-prepared GO can be used as a high-efficiency adsorbent for lead-containing wastewater.

Keywords: graphene oxide; attapulgite; lead ion; adsorption

1. Introduction

Pb²⁺ is a heavy metal ion found in industrial and agricultural wastewater and acidic landfill leachate [1]. Because of its high toxicity, nonbiodegradability, wide presence, and bioaccumulation, it constitutes a pollutant that threatens humans and the environment [2]. Long-term consumption of lead-ion-containing drinking water can induce serious diseases, such as anemia, reproductive diseases, genotoxicity, and nervous system effects. In particular, children bear the greatest risk of lead-induced toxicity [3]. These concerns have caused increasingly more scientists to investigate simple yet highly effective treatment methods for lead-containing wastewater [4]. Methods that have been used to date in the removal of lead ions from wastewater include chemical precipitation [5], coprecipitation [6], cloud-point extraction [7], electrochemical reduction [8], flocculation [9], ion exchange [10], membrane filtration [11,12], and adsorption [2–4,13–16]. Among these methods, adsorption offers the advantages of simple operation, high efficiency, and economic feasibility, and environmental friendliness [17]. However, it is essential to identify high-efficiency adsorbents that are easy to prepare, inexpensive, and easy to regenerate. Most studies have focused on the search for these high-efficiency adsorbents.

Graphene oxide (GO) is typically obtained by oxidation or sonication of graphite, and it possesses oxygen-containing functional groups, including hydroxyl groups (–OH), epoxy groups (–C=O), and carboxyl groups (–COOH). In addition, GO also possesses a high specific surface area [18]. Compared to other carbon-based materials, GO exhibits better environmental compatibility and biocompatibility [19]. Oxygen-containing functional groups can be used as the adsorption sites for heavy metal ions in wastewater [20]. Through interaction with these oxygen-containing functional groups, heavy metal ions can be removed from wastewater, thus enabling purification [21]. In addition, the presence of these functional groups enables the stable dispersion of GO in water and other polar organic solvents [22]. However, pure GO or GO-based adsorbents reported in the literature have suffered from limitations such as toxic preparation conditions, complex preparation methods, difficulty in separation, and high cost. As a result, inorganic clay minerals with excellent adsorption

and separation properties are selected here to create a composite with GO to fabricate Pb^{2+} adsorbents with excellent properties at a low cost.

Attapulgite (ATP) is a water-containing magnesium aluminum phyllosilicate, which is an inorganic mineral that exhibits high cation exchange capacity, rapid hydration [23], and environmental compatibility. Research has shown that the as-prepared GO composites exhibit excellent adsorption to heavy metal ions such as Pb^{2+} , Zn^{2+} , Cu^{2+} , Cd^{2+} [24], and Ni^{2+} [25]. ATP can be regenerated after adsorption saturation. In addition, because of its low cost and easy access [26], ATP exhibits wide application potential and practical value in the removal of heavy metal ions in wastewater due to its cheapness, abundance, and chemical stability [27].

Although there are abundant studies of GO composite materials [28], there are no reports on facile composite materials combining GO and the inorganic clay material ATP. GO exhibits a two-dimensional layer structure [29], whereas the ATP single crystal exhibits a fine fibrous morphology [30]. The present study aimed to graft ATP to the GO surface, forming a novel composite material with a “plane-needle” structure, thus achieving improved GO properties and decreased cost in the treatment of lead-containing wastewater. The already large specific surface area of GO was further increased to improve the separation performance, thus avoiding the loss of GO nanoparticles in lead-containing wastewater and achieving more efficient and economical treatment of heavy metal lead ions in wastewater.

2. Materials and Methods

2.1. Materials

GO in liquid form with a concentration of 2 mg/mL was purchased from Nano Technology Co., Ltd. ATP was purchased from Anhui Mingguang ATP Clay Factory. Other reagents were of analytical or guaranteed grade, and deionized (DI) water was generated in the lab. Pb^{2+} stock solution was obtained by dissolving $\text{Pb}(\text{NO}_3)_2$ in DI water.

2.2. Methods

2.2.1. Preparation of the As-Prepared GO Composite

GO was reacted with ATP in two steps. First, 50 g ATP was dissolved in 1000 mL DI water and immersed for 24 h. Then, 1 g of 2% sodium hexametaphosphate was added to the above solution. The resulting solution was stirred under magnetic stirring for 2 h and allowed to stand stationary for 2–3 h until a stable separation of liquid was observed. The upper suspension was removed to a volumetric flask, and water was added to a final volume of 1 L in the volumetric flask; the precipitate at the bottom of the beaker was then dried and weighed. The concentration of the 1 L suspension solution was calculated, and the suspension solution was then diluted to a concentration of 4 mg/mL. Second, 100 mL of 2 mg/mL GO and 100 mL of 4 mg/mL ATP were sonicated individually at 1200 W for 1 h, and the two solutions were mixed and sonicated at 80 W for 3 h. The sonicated mixture solution was then stirred at 120 r/min on a magnetic stirrer for 10 h at 45 °C. The chemical reaction between ATP and GO is shown in Figure 1.

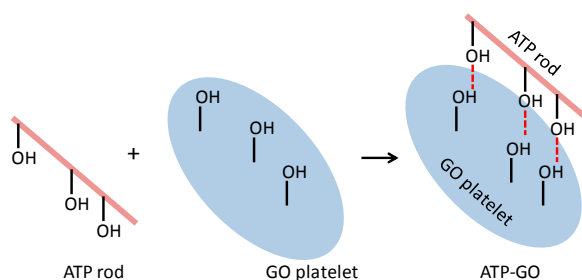


Figure 1. Illustration of the reaction between graphene oxide (GO) and attapulgite (ATP).

2.2.2. Characterization

The sample morphology was characterized by scanning electron microscopy (SEM, Carl Zeiss group, Germany), transmission electron microscopy (TEM, TECNAIG2 TF20, Thermo Fisher Scientific, USA), and X-ray photoelectron spectroscopy (XPS, Phi5702, Al target excitation source, Physical Electronics Inc., USA). Fourier transform infrared spectroscopy (FTIR, IR Prestige-21, Shimadzu, Japan) was used to analyze the IR spectra of samples at room temperature in the wavenumber range of 4000~400 cm^{-1} using KBr as the background.

2.2.3. Adsorption Experiment

In the adsorption experiments, the adsorbent solution and Pb^{2+} stock solution were mixed, and then DI water was added to obtain 0.3 mg/mL adsorbent and 150 mg/L Pb^{2+} . The pH value was 5, which was adjusted by 0.1 mol/L HCl and 0.1 mol/L NaOH. The reaction mixture was stirred 2 h at 298 K followed by centrifuged at 6000 r/min for 10 min. The concentration of Pb^{2+} in the supernatant was measured using an atomic absorption spectrophotometer (Spectra AA110/220, Varian Inc., Palo Alto, PA, USA). All experimental data were the average of three parallel experiments. The removal efficiency of Pb^{2+} was calculated using the following equation:

$$\eta = \frac{C_0 - C_e}{C_0} \times 100\% \quad (1)$$

where C_0 and C_e are the initial and equilibrium concentrations of Pb^{2+} in mg/L; and η is the removal efficiency in %.

To compare the adsorption capacity, the initial concentration of Pb^{2+} was 100 mg/L. To investigate the pH effects on Pb removal, the pH was adjusted from 3~9. To examine the contact time effects on Pb removal, the solution was stirred for 5 to 120 min. To evaluate the initial concentration on Pb^{2+} removal, Pb^{2+} dosage varied from 20 mg/L to 160 mg/L. The experiments were conducted at 298 K, 308 K, and 318 K to investigate the thermodynamic models. To investigate the regeneration and recycling properties of the as-prepared GO, HCl solution was used as the regenerate; the concentration was varied from 0.2 to 0.3, 0.5, 0.8, and 1.2 mol/L.

3. Results and Discussion

3.1. Characterization

The SEM and TEM images of ATP, GO, and the prepared GO are shown in Figure 2. Figure 2a shows that the purified ATP exhibited a rod-like morphology and a typical fibrous structure and easily aggregated to form clusters. Figure 2b indicates that the GO exhibited a layer structure that was folded at the edges. In addition, many layers were stacked together because the chemical bond between GO layers easily led to aggregation. Figure 2c shows that ATP was uniformly intercalated on the GO surface. The presence of ATP changed the stacking behavior of pure GO, and the presence of GO resulted in the uniform distribution of ATP. The weakening of aggregate stacking and the appearance of homogenization and uniformity increased the surface area of the as-prepared GO considerably, thus producing more adsorption sites to aid in the removal of heavy metals. The results indicated that the ATP and GO were very well mixed. Figure 2d shows that GO exhibited a transparent, thin film structure and that folds were found on the edges, in agreement with the SEM results. It can be observed from the comparison of the TEM images of GO in Figure 2e that ATP was present and uniformly distributed on the GO surface, further indicating successful fabrication of the as-prepared GO composite. That is, a simple hydrothermal reaction can be used to prepare the as-prepared GO composite adsorbent.

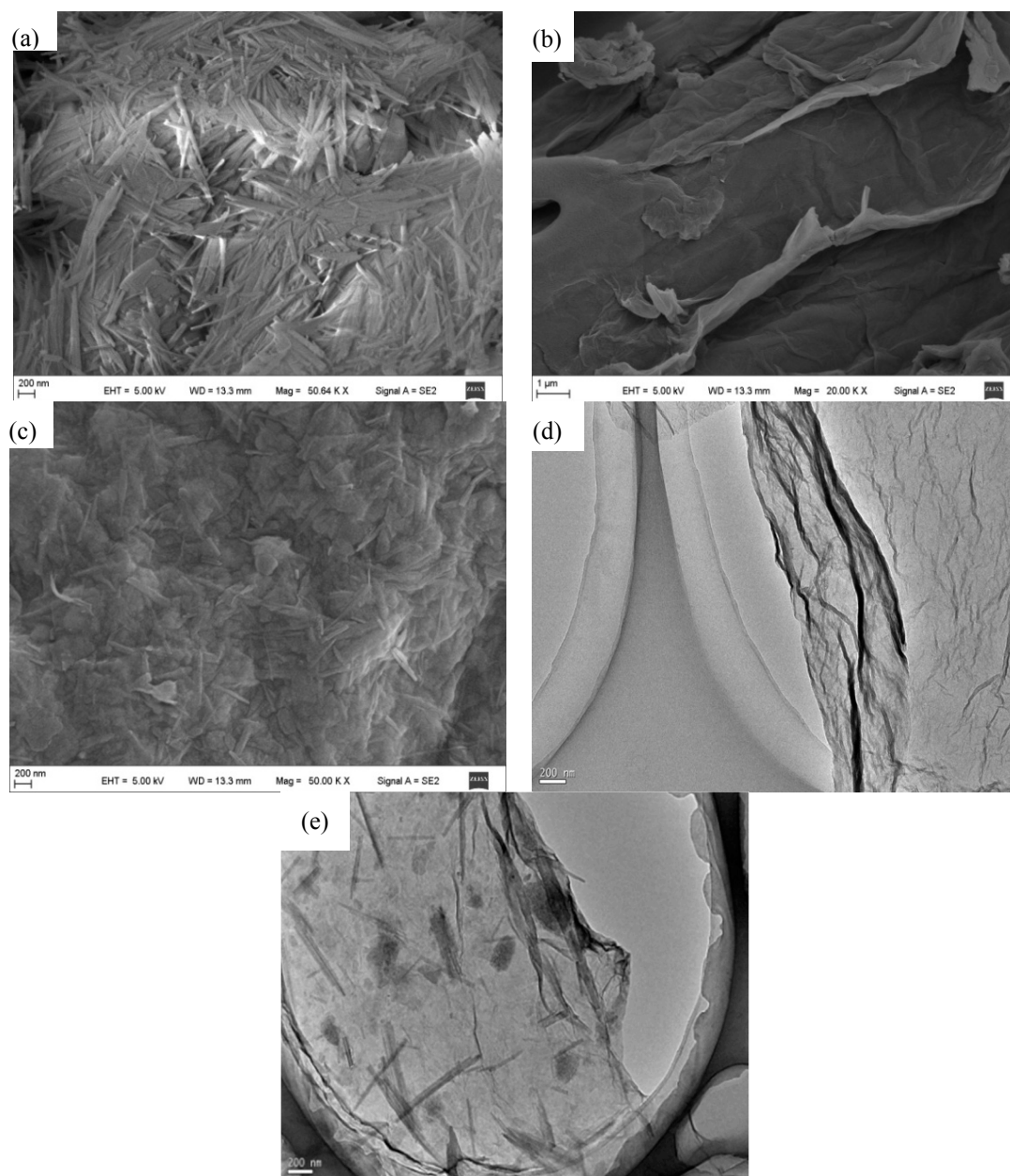


Figure 2. Scanning electron microscopy (SEM) and transmission electron microscopy (TEM) images of (a) ATP, (b) GO, (c) as-prepared GO and TEM images of (d) GO and (e) as-prepared GO.

Figure 3 shows the FTIR spectra of GO, ATP, and the as-prepared GO. In the FTIR spectrum of GO, the peaks at 1110 cm^{-1} , 1400 cm^{-1} , and 1629 cm^{-1} correspond to the C–O–C vibration, C–OH vibration, and C–C vibration, respectively, in the sp^2 hybridized carbon skeleton; the peaks at 1732 cm^{-1} and 3149 cm^{-1} correspond to the C–O and O–H vibrations in –COOH, further revealing the presence of carboxyl, epoxide, and hydroxyl groups in GO [31]. The FTIR spectrum of ATP indicates that the appearance of the broad peak at $3550\text{ cm}^{-1}\sim 3616\text{ cm}^{-1}$ was due to the stretching vibrations of (Al)O–H and (Mg)O–H, which, however, shifted to lower wavenumbers in the FTIR spectrum of the as-prepared GO, suggesting the existence of hydrogen bonding between ATP and GO. The absorption peaks at 729 cm^{-1} and 796 cm^{-1} in the FTIR spectra of ATP and the as-prepared GO are attributed to the stretching vibration of Si–O. Evidently, the Si–O in ATP was transferred to the as-prepared GO [32]. Thus, ATP was successfully intercalated onto the GO surface, forming a novel adsorbent for heavy metals.

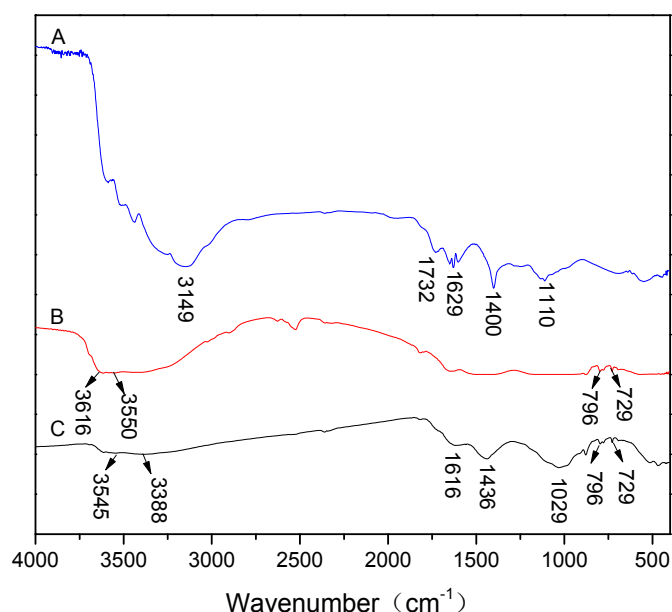


Figure 3. Fourier transform infrared spectroscopy (FTIR) spectra of (A) GO, (B) ATP, and (C) as-prepared GO.

The main chemical compositions are SiO_2 , MgO , Al_2O_3 , and contain a certain amount of Fe_2O_3 , CaO , K_2O , MnO , Na_2O , and TiO_2 , which vary from places of origin [33]. Figure 4 shows the XPS spectra of GO and the prepared GO. By comparing the XPS spectrum of GO with that of the as-prepared GO, the peaks of Mg 2p, Al 2p, and Si 2p appeared at 54 eV, 78 eV, and 104 eV, respectively, in the spectrum of the as-prepared GO, indicating that ATP, a material rich in magnesium aluminum phyllosilicate, can form a composite adsorbent with GO. The elemental compositions of GO revealed the presence of C and O; however, for the as-prepared GO, in addition to C and O, the presence of Mg, Al, Si, Ca, and Fe further suggests that the reaction combined ATP and GO, thus forming a novel composite adsorption material.

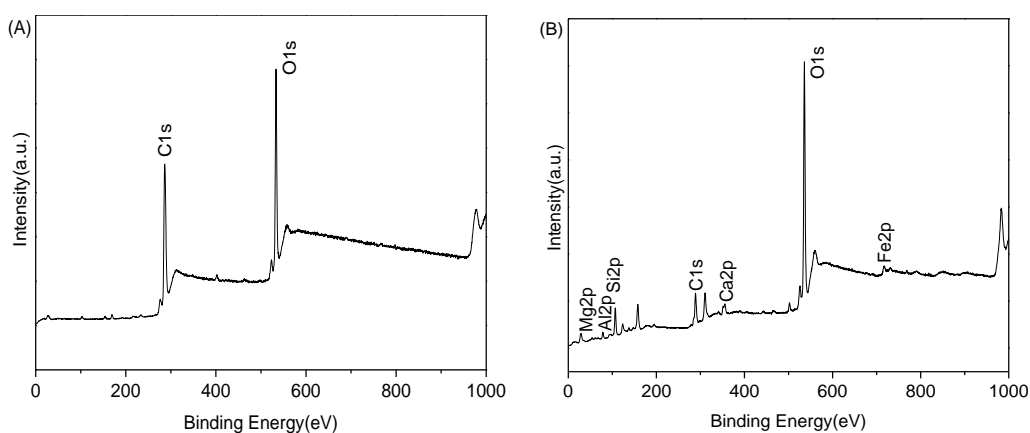


Figure 4. X-ray photoelectron spectroscopy (XPS) spectra of (A) GO and (B) as-prepared GO.

3.2. Comparison of Adsorbents

To compare the adsorption properties of as-prepared GO with those of pure GO and ATP on adsorption, GO, ATP, and as-prepared GO were chosen in the adsorption experiments, as shown in Figure 5. ATP was obtained by purification; GO was used as received. Figure 5 indicates that the removal of Pb^{2+} was 308.7 mg/g as-prepared GO, compare to 124.7 mg/g GO and 72.7 mg/g ATP. GO has high adsorption capacity—it is difficult to separate from water by centrifugation—and other

researchers rely mainly on filtration for separation. The adsorption capacity of ATP is far less than GO, while it easy separate by centrifugation due to its very high density. for the as-prepared GO, the high adsorption capacity of GO and the ease of separation of ATP were brought into play.

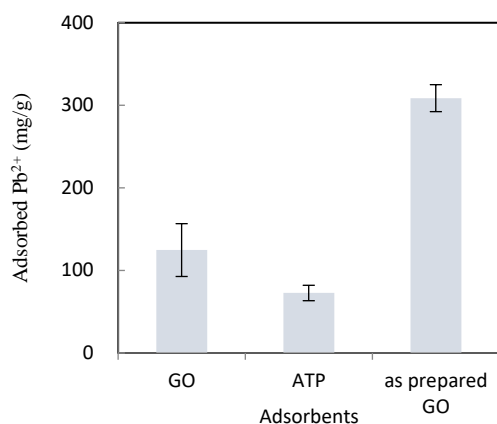


Figure 5. Removal efficiencies of GO, ATP, and as-prepared GO.

The adsorption capacity of Pb²⁺ on as-prepared GO is greater than the 62.1 mg/g adsorption on attapulgite [33], and far greater than 23~27 mg/g adsorption obtained on zeolite [34] and zeolite-type [35] adsorbents.

3.3. Effect of pH

The pH affects not only the charge and state of functional groups on the surface of the as-prepared GO, but also the ionic state of Pb in aqueous solution [36]. The optimal pH is different for the adsorption of different heavy metals. The pH in the adsorption of Pb²⁺ on the as-prepared GO varied from 3 to 9; the results are shown in Figure 6. The contact time was 2 h to ensure that adsorption reached equilibrium. Figure 6 indicates that at a low pH value of 3, the oxygen-containing functional groups on the as-prepared GO surface were protonated. Consequently, because of electrostatic repulsion, the positively charged surface of the adsorbent did not complex well with Pb²⁺, thus resulting in a low removal efficiency. When the pH was increased to 5, the degree of protonation of the oxygen-containing functional groups was weak, directly resulting in an increase in removal efficiency to 90%. When the pH was increased to 6, a precipitation reaction was initiated, thus maintaining the removal efficiency at approximately 99%. In fact, the main states of lead in aqueous solution include Pb²⁺, Pb(OH)⁺, Pb(OH)₂, Pb(OH)₃⁻, and Pb(OH)₄²⁻ [37]. When pH < 6, Pb²⁺ is the primary form. Therefore, a pH value of 5 was chosen for the subsequent adsorption experiments of Pb²⁺.

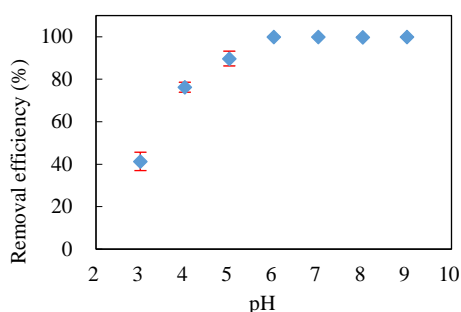


Figure 6. Effect of the solution pH on the adsorption of Pb²⁺ by the as-prepared GO, C₀ = 150 mg/L, m/v = 0.3 g/L, t = 2 h, and T = 298 K.

3.4. Adsorption Kinetics

The effects of adsorption time on the removal efficiency of Pb^{2+} at pH 5.0 are shown in Figure 7. The adsorption of Pb^{2+} on the as-prepared GO increased significantly with an increasing reaction time of 100 min. Different adsorption kinetic models exist to describe adsorption mechanisms, including the pseudo-first-order kinetics model [38,39] and the pseudo-second-order kinetics model [40], which can be represented as follows:

$$\frac{q_t}{q_e} = 1 - e^{-k_1 t} \quad (2)$$

$$\frac{t}{q_t} = \frac{1}{k_2 q_e^2} + \frac{1}{q_e} t \quad (3)$$

where q_e is the equilibrium adsorption capacity in mg/g, q_t is the adsorption capacity at time t in mg/g, and k_1 (min^{-1}) and k_2 ($\text{g}/(\text{mg}\cdot\text{min})$) are the rate constants of the pseudo-first-order and pseudo-second-order kinetics models, respectively.

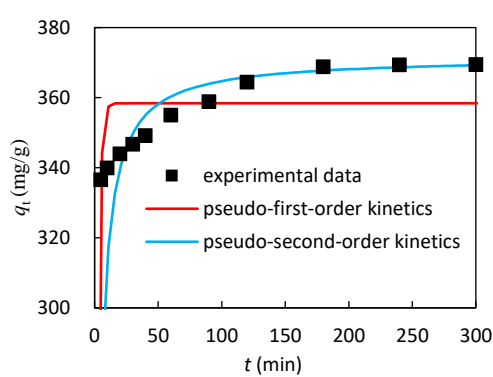


Figure 7. Adsorption kinetics of Pb^{2+} on the as-prepared GO, $C_0 = 150$ mg/L, pH = 5.0, $m/v = 0.3$, and $T = 298$ K.

By nonlinear fitting, the fitting parameters of the pseudo-first-order model are $k_1 = 0.5398$ min^{-1} , q_e is 358.40 mg/g and R^2 is 0.5202, and the fitting parameters of the pseudo-second-order model are $k_2 = 0.001438$ $\text{g}/(\text{mg}\cdot\text{min})$, q_e is 371.54 mg/g, and R^2 is 0.8312. It can be observed that the pseudo-second-order model is a better fit to the adsorption results of Pb^{2+} by the as-prepared GO, further suggesting that the adsorption rate depends primarily on chemisorption [4]. This result reveals that in addition to the formation of chemical bonds, the transfer and exchange of electrons occur in the adsorption reaction. In the initial 5 min, chemisorption was rapid, thus leading to a rapid increase in the adsorption reaction rate.

3.5. Adsorption Isotherm

The Langmuir isotherm equation [41] and the Freundlich isotherm equation [42] were used to fit the equilibrium of the experimental data, as shown in Figure 8 and Table 1:

$$q_e = \frac{q_{\max} K_L C_e}{1 + K_L C_e} \quad (4)$$

$$q_e = K_f C_e^{\frac{1}{n}} \quad (5)$$

where C_e is the equilibrium concentration in mg/L, q_e is the equilibrium adsorption capacity in mg/g, k_L is the constant of the Langmuir model in L/mg, q_{\max} is the maximum theoretical adsorption capacity in mg/g, and K_f and n are the adsorption capacity and adsorption strength of the Freundlich model, respectively.

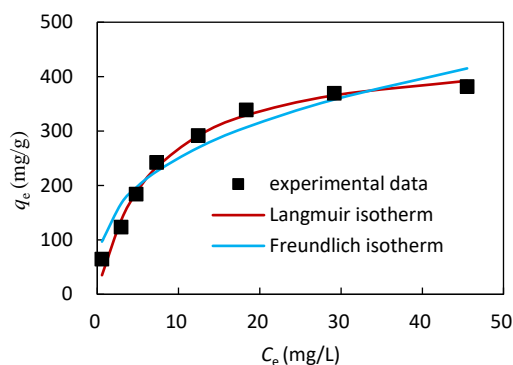


Figure 8. Comparison experimental data and two isotherm equations for Pb²⁺ adsorption on the as-prepared GO at 298 K.

Table 1. Parameters of Langmuir and Freundlich adsorption isotherm models for Pb²⁺ on as-prepared GO.

Langmuir			Freundlich		
q_{max} (mg/g)	K_L (L/mg)	R^2	K_F (mg/g)	n	R^2
450.9	0.147	0.9925	116.5	3.005	0.9127

By nonlinear fitting, the fitting parameter q_{max} of the Langmuir isothermal adsorption equation is 450.9 mg/g with $k_L = 0.147$ L/mg and $R^2 = 0.9925$, while the R^2 of Freundlich is 0.9127 with $k_F = 116.5$ mg/g and $n = 3.005$. This result indicates that the adsorption process is in better agreement with the Langmuir isothermal adsorption equation than with the Freundlich equation and that the adsorption occurs through homogeneous monolayer adsorption. The maximum adsorption capacity is 450.9 mg/g.

3.6. Thermodynamic Parameters

The thermodynamic parameters ΔH^0 , ΔG^0 , and ΔS^0 of Pb²⁺ adsorption on the as-prepared GO can be calculated according to the temperature adsorption isotherms. The standard free energy, ΔG^0 , can be obtained by the following equation [43]:

$$\Delta G^0 = -RT \ln K_0 = \Delta H^0 - T \Delta S^0 \tag{6}$$

where R is the universal gas constant, 8.314 J/(mol·K), and T is the absolute temperature in K. K_0 is the thermodynamic equilibrium constant in mg/L, which can be calculated by q_e/C_e . Based on Equation (6), the standard enthalpy change, ΔH^0 , and standard entropy change, ΔS^0 , can be obtained from the slope and intercept of the plot of $\ln K_0$ vs. $1/T$ by the following equation:

$$\ln K_0 = \frac{\Delta S^0}{R} - \frac{\Delta H^0}{RT} \tag{7}$$

By calculation, the negative values of ΔG^0 are -4.19 kJ/mol at 298 K, -4.68 kJ/mol at 308 K, and -5.78 kJ/mol at 318 K, indicating that adsorption of Pb²⁺ by the as-prepared GO is a spontaneous process [44,45]. ΔH^0 is 19.40 kJ/mol, and ΔS^0 is 78.17 J/(mol·K), indicating that the adsorption of Pb²⁺ by the as-prepared GO is an exothermic process [46].

3.7. Regeneration and Recycling

The HCl concentration effect on the desorption of Pb²⁺ from the adsorbed as-prepared GO is shown in Figure 9. After selecting the optimum concentration, this concentration was used to investigate the adsorption and desorption rates of the adsorbents in recycling.

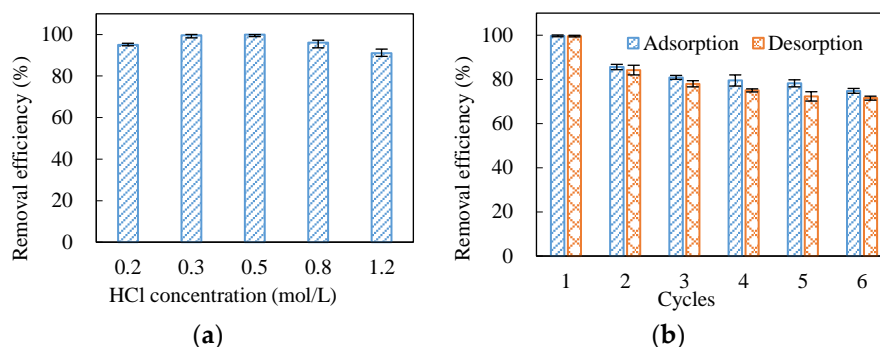


Figure 9. (a) Effect of HCl concentration on the desorption capacity of Pb²⁺; (b) adsorption–desorption cycles ($C_0 = 100$ mg/L, $m/v = 0.3$ g/L, the HCl concentration is 0.5 mol/L, $T = 298$ K).

Figure 9 indicates that the desorption rate of Pb²⁺ by the HCl solution with a concentration of 0.2, 0.3, 0.5, 0.8, and 1.2 mol/L was greater than 91% in all cases, indicating that HCl can be used as a regenerator for the desorption of Pb²⁺ from the as-prepared GO. The desorption rate increased gradually with increasing HCl concentration; 0.5 mol/L of HCl solution exhibited the best desorption effect. When the concentration of the HCl was 0.2 mol/L, the concentration of H⁺ was low, and it could not fully exchange Pb²⁺ adsorbed on the prepared GO surface. When the concentration of the HCl solution reached 0.3 mol/L, the concentration of H⁺ increased; consequently, the exchange amount of Pb²⁺ increased, and the desorption rate improved. However, when the concentration of HCl increased to between 0.8 and 1.2 mol/L, the desorption rate was not as high, maybe because a high acid concentration resulted in destruction of the structure of the composite material, thus leading to a decrease in the desorption rate. The adsorption rate was 74.8% of the initial rate after six adsorption–desorption cycles, indicating that the prepared GO exhibits a high recycling efficiency and offers practical value for use in wastewater treatment areas.

4. Conclusions

The as-prepared GO is an easy-to-produce and low-cost heavy metal adsorbent that can be prepared by a simple hydrothermal intercalation reaction of ATP and GO. Compared to other types of adsorbents and GO-based adsorbents reported in the literature, the prepared GO exhibits excellent adsorption and separation properties. The maximum adsorption capacity of Pb²⁺ on as-prepared GO at pH 5 and 25 °C was 450.9 mg/g. The adsorption–desorption experiments indicate that high concentrations of HCl solution can destroy the structure of the composite adsorption material. Low concentrations of HCl, however, can improve the desorption rates. The composite adsorbent retains a high removal efficiency of lead ions after six adsorption–desorption cycles and can be used in the treatment and purification of heavy metal-containing wastewater.

Author Contributions: B.W. designed the research and wrote original draft preparation, X.C. and G.W. collected samples and conducted experiments, H.L. and X.S. conducted experiments and analyzed samples, L.D. conceptualized and reviewed the paper.

Funding: This research received no external funding.

Acknowledgments: This work was supported by the National Natural Science Foundation of China (No. 51668032), the Foundation of a Hundred Youth Talents Training Program of Lanzhou Jiaotong University (No. 152022) and the Natural Science Foundation of Gansu Province of China (No. 145RJZA209).

Conflicts of Interest: The authors declare no conflict of interest. The funders had no role in the design of the study; in the collection, analyses, or interpretation of data; in the writing of the manuscript, or in the decision to publish the results.

References

1. Hudcová, B.; Veselská, V.; Filip, J.; Číhalová, S.; Komárek, M. Highly effective Zn(II) and Pb(II) removal from aqueous solutions using Mg-Fe layered double hydroxides: Comprehensive adsorption modeling coupled with solid state analyses. *J. Clean. Prod.* **2018**, *171*, 944–953. [[CrossRef](#)]
2. Saeidi, N.; Parvini, M.; Niavarani, Z. High surface area and mesoporous graphene/activated carbon composite for adsorption of Pb(II) from wastewater. *J. Environ. Chem. Eng.* **2015**, *3 Pt A*, 2697–2706. [[CrossRef](#)]
3. Thanh, H.T.M.; Phuong, T.T.T.; Hang, P.T.L.; Toan, T.T.T.; Tuyen, T.N.; Mau, T.X.; Khieu, D.Q. Comparative study of Pb(II) adsorption onto MIL-101 and Fe-MIL-101 from aqueous solutions. *J. Environ. Chem. Eng.* **2018**, *6*, 4093–4102. [[CrossRef](#)]
4. Cui, L.; Wang, Y.; Gao, L.; Hu, L.; Yan, L.; Wei, Q.; Du, B. EDTA functionalized magnetic graphene oxide for removal of Pb(II), Hg(II) and Cu(II) in water treatment: Adsorption mechanism and separation property. *Chem. Eng. J.* **2015**, *281*, 1–10. [[CrossRef](#)]
5. Meunier, N.; Drogui, P.; Montané, C.; Hausler, R.; Mercier, G.; Blais, J.-F. Comparison between electrocoagulation and chemical precipitation for metals removal from acidic soil leachate. *J. Hazard. Mater.* **2006**, *137*, 581–590. [[CrossRef](#)] [[PubMed](#)]
6. Tufekci, M.; Bulut, V.N.; Elvan, H.; Ozdes, D.; Soylak, M.; Duran, C. Determination of Pb(II), Zn(II), Cd(II), and Co(II) ions by flame atomic absorption spectrometry in food and water samples after preconcentration by coprecipitation with Mo(VI)-diethyldithiocarbamate. *Environ. Monit. Assess.* **2013**, *185*, 1107–1115. [[CrossRef](#)] [[PubMed](#)]
7. Kazi, T.G.; Shah, F.; Afridi, H.I.; Khan, S.; Arian, S.S.; Brahman, K.D. A green preconcentration method for determination of cobalt and lead in fresh surface and waste water samples prior to flame atomic absorption spectrometry. *J. Anal. Methods Chem.* **2012**, *2012*, 713862. [[CrossRef](#)]
8. Liu, Y.; Yan, J.; Yuan, D.; Li, Q.; Wu, X. The study of lead removal from aqueous solution using an electrochemical method with a stainless steel net electrode coated with single wall carbon nanotubes. *Chem. Eng. J.* **2013**, *218*, 81–88. [[CrossRef](#)]
9. Feng, J.; Yang, Z.; Zeng, G.; Huang, J.; Xu, H.; Zhang, Y.; Wei, S.; Wang, L. The adsorption behavior and mechanism investigation of Pb(II) removal by flocculation using microbial flocculant GA1. *Bioresour. Technol.* **2013**, *148*, 414–421. [[CrossRef](#)]
10. Inglezakis, V.J.; Loizidou, M.D.; Grigoropoulou, H.P. Ion exchange of Pb²⁺, Cu²⁺, Fe³⁺, and Cr³⁺ on natural clinoptilolite: Selectivity determination and influence of acidity on metal uptake. *J. Colloid Interface Sci.* **2003**, *261*, 49–54. [[CrossRef](#)]
11. Oehmen, A.; Vergel, D.; Fradinho, J.; Reis, M.A.M.; Crespo, J.G.; Velizarov, S. Mercury removal from water streams through the ion exchange membrane bioreactor concept. *J. Hazard. Mater.* **2014**, *264*, 65–70. [[CrossRef](#)]
12. Madaeni, S.S.; Heidary, F.; Salehi, E. Co-adsorption/filtration of heavy metal ions from water using regenerated cellulose UF membranes modified with DETA ligand. *Sep. Sci. Technol.* **2013**, *48*, 1308–1314. [[CrossRef](#)]
13. Liu, Y.; Xu, L.; Liu, J.; Liu, X.; Chen, C.; Li, G.; Meng, Y. Graphene oxides cross-linked with hyperbranched polyethylenimines: Preparation, characterization and their potential as recyclable and highly efficient adsorption materials for lead(II) ions. *Chem. Eng. J.* **2016**, *285*, 698–708. [[CrossRef](#)]
14. Zhang, J.; Gong, J.-L.; Zenga, G.-M.; Ou, X.-M.; Jiang, Y.; Chang, Y.-N.; Guo, M.; Zhang, C.; Liu, H.-Y. Simultaneous removal of humic acid/fulvic acid and lead from landfill leachate using magnetic graphene oxide. *Appl. Surf. Sci.* **2016**, *370*, 335–350. [[CrossRef](#)]
15. Fan, L.; Luo, C.; Sun, M.; Li, X.; Qiu, H. Highly selective adsorption of lead ions by water-dispersible magnetic chitosan/graphene oxide composites. *Colloids Surf. B Biointerfaces* **2013**, *103*, 523–529. [[CrossRef](#)] [[PubMed](#)]
16. Luo, S.; Xu, X.; Zhou, G.; Liu, C.; Tang, Y.; Liu, Y. Amino siloxane oligomer-linked graphene oxide as an efficient adsorbent for removal of Pb(II) from wastewater. *J. Hazard. Mater.* **2014**, *274*, 145–155. [[CrossRef](#)]
17. Fu, F.; Wang, Q. Removal of heavy metal ions from wastewaters: A review. *J. Environ. Manag.* **2011**, *92*, 407–418. [[CrossRef](#)]

18. Montes-Navajas, P.; Asenjo, N.G.; Santamaría, R.; Menéndez, R.; Corma, A.; García, H. Surface area measurement of graphene oxide in aqueous solutions. *Langmuir* **2013**, *29*, 13443–13448. [[CrossRef](#)] [[PubMed](#)]
19. Chen, L.; Hu, P.; Zhang, L.; Huang, S.; Luo, L.; Huang, C. Toxicity of graphene oxide and multi-walled carbon nanotubes against human cells and zebrafish. *Sci. China Chem.* **2012**, *55*, 2209–2216. [[CrossRef](#)]
20. Chen, H.; Gao, B.; Li, H. Removal of sulfamethoxazole and ciprofloxacin from aqueous solutions by graphene oxide. *J. Hazard. Mater.* **2015**, *282*, 201–207. [[CrossRef](#)]
21. Gu, D.; Fein, J.B. Adsorption of metals onto graphene oxide: Surface complexation modeling and linear free energy relationships. *Colloids Surf. A Physicochem. Eng. Asp.* **2015**, *481*, 319–327. [[CrossRef](#)]
22. Paredes, J.; Villar-Rodil, S.; Martínez-Alonso, A.; Tascon, J. Graphene oxide dispersions in organic solvents. *Langmuir* **2008**, *24*, 10560–10564. [[CrossRef](#)] [[PubMed](#)]
23. Liu, Y.; Kang, Y.; Mu, B.; Wang, A. Attapulgite/bentonite interactions for methylene blue adsorption characteristics from aqueous solution. *Chem. Eng. J.* **2014**, *237*, 403–410. [[CrossRef](#)]
24. Zhu, L.; Zhang, L.; Tang, Y.; Kou, X. Synthesis of sodium alginate graft poly (acrylic acid-co-2-acrylamido-2-methyl-1-propane sulfonic acid)/attapulgite hydrogel composite and the study of its adsorption. *Polym. Plast. Technol. Eng.* **2014**, *53*, 74–79. [[CrossRef](#)]
25. Wang, W.; Wang, J.; Wang, A. pH-Responsive nanocomposites from methylcellulose and attapulgite nanorods: Synthesis, swelling and absorption performance on heavy metal ions. *J. Macromol. Sci. Part A* **2012**, *49*, 306–315. [[CrossRef](#)]
26. Wang, J.; Han, X.; Ma, H.; Ji, Y.; Bi, L. Adsorptive removal of humic acid from aqueous solution on polyaniline/attapulgite composite. *Chem. Eng. J.* **2011**, *173*, 171–177. [[CrossRef](#)]
27. De Gisi, S.; Lofrano, G.; Grassi, M.; Notarnicola, M. Characteristics and adsorption capacities of low-cost sorbents for wastewater treatment: A review. *Sustain. Mater. Technol.* **2016**, *9*, 10–40. [[CrossRef](#)]
28. Chen, X.; Chen, B. Facile fabrication of crumpled graphene oxide nanosheets and its Platinum nanohybrids for high efficient catalytic activity. *Environ. Pollut.* **2018**, *243*, 1810–1817. [[CrossRef](#)] [[PubMed](#)]
29. Tan, L.; Wang, S.; Du, W.; Hu, T. Effect of water chemistries on adsorption of Cs(I) onto graphene oxide investigated by batch and modeling techniques. *Chem. Eng. J.* **2016**, *292*, 92–97. [[CrossRef](#)]
30. Bradley, W. The structural scheme of attapulgite. *Am. Mineral.* **1940**, *25*, 405–410.
31. Fan, L.; Luo, C.; Li, X.; Lu, F.; Qiu, H.; Sun, M. Fabrication of novel magnetic chitosan grafted with graphene oxide to enhance adsorption properties for methyl blue. *J. Hazard. Mater.* **2012**, *215–216*, 272–279. [[CrossRef](#)] [[PubMed](#)]
32. Zhang, J.; Wang, Q.; Wang, A. Synthesis and characterization of chitosan-g-poly(acrylic acid)/attapulgite superabsorbent composites. *Carbohydr. Polym.* **2007**, *68*, 367–374. [[CrossRef](#)]
33. Potgieter, J.H.; Potgieter-Vermaak, S.S.; Kalibantonga, P.D. Heavy metals removal from solution by palygorskite clay. *Miner. Eng.* **2006**, *19*, 463–470. [[CrossRef](#)]
34. Wang, S.; Ariyanto, E. Competitive adsorption of malachite green and Pb ions on natural zeolite. *J. Colloid Interface Sci.* **2007**, *314*, 25–31. [[CrossRef](#)]
35. Xing, P.; Wang, C.; Ma, B.; Chen, Y. Removal of Pb(II) from aqueous solution using a new zeolite-type absorbent: Potassium ore leaching residue. *J. Environ. Chem. Eng.* **2018**, *6*, 7138–7143. [[CrossRef](#)]
36. Liao, B.; Sun, W.-Y.; Guo, N.; Ding, S.-L.; Su, S.-J. Equilibriums and kinetics studies for adsorption of Ni (II) ion on chitosan and its triethylenetetramine derivative. *Colloids Surf. A Physicochem. Eng. Asp.* **2016**, *501*, 32–41. [[CrossRef](#)]
37. Huang, X.; Pan, M. The highly efficient adsorption of Pb (II) on graphene oxides: A process combined by batch experiments and modeling techniques. *J. Mol. Liq.* **2016**, *215*, 410–416. [[CrossRef](#)]
38. O’Shannessy, D.J.; Winzor, D.J. Interpretation of Deviations from Pseudo-First-Order Kinetic Behavior in the Characterization of Ligand Binding by Biosensor Technology. *Anal. Biochem.* **1996**, *236*, 275–283. [[CrossRef](#)] [[PubMed](#)]
39. Derylo-Marczewska, A.; Blachnio, M.; Marczewski, A.W.; Seczkowska, M.; Tarasiuk, B. Phenoxycid pesticide adsorption on activated carbon—Equilibrium and kinetics. *Chemosphere* **2019**, *214*, 349–360. [[CrossRef](#)]
40. Ho, Y.-S. Second-order kinetic model for the sorption of cadmium onto tree fern: A comparison of linear and non-linear methods. *Water Res.* **2006**, *40*, 119–125. [[CrossRef](#)]
41. Lanowix, I. The adsorption of gases on plane surface of glass, mica and platinum. *J. Am. Chem. Soc.* **1918**, *30*, 1361–1403.
42. Freundlich, U. Die adsorption in lusungen. *Phys. Chem.* **1906**, *57*, 385–470.

43. Liu, L.; Li, C.; Bao, C.; Jia, Q.; Xiao, P.; Liu, X.; Zhang, Q. Preparation and characterization of chitosan/graphene oxide composites for the adsorption of Au(III) and Pd(II). *Talanta* **2012**, *93*, 350–357. [[CrossRef](#)]
44. Niwas, R.; Gupta, U.; Khan, A.A.; Varshney, K.G. The adsorption of phosphamidon on the surface of styrene supported zirconium (IV) tungstophosphate: A thermodynamic study. *Colloids Surf. A Physicochem. Eng. Asp.* **2000**, *164*, 115–119. [[CrossRef](#)]
45. Wang, Y.; Wang, X.; Wang, X.; Liu, M.; Yang, L.; Wu, Z.; Xia, S.; Zhao, J. Adsorption of Pb (II) in aqueous solutions by bamboo charcoal modified with KMnO_4 via microwave irradiation. *Colloids Surf. A Physicochem. Eng. Asp.* **2012**, *414*, 1–8. [[CrossRef](#)]
46. Li, Y.-H.; Di, Z.; Ding, J.; Wu, D.; Luan, Z.; Zhu, Y. Adsorption thermodynamic, kinetic and desorption studies of Pb^{2+} on carbon nanotubes. *Water Res.* **2005**, *39*, 605–609. [[CrossRef](#)] [[PubMed](#)]



© 2019 by the authors. Licensee MDPI, Basel, Switzerland. This article is an open access article distributed under the terms and conditions of the Creative Commons Attribution (CC BY) license (<http://creativecommons.org/licenses/by/4.0/>).